Analysis of Three-Dimensional Turbulent Wakes by a Momentum Integral Technique

B. Lakshminarayana* and J. Zhang†
Pennsylvania State University, University Park, Pennsylvania

A momentum integral technique has been developed for prediction of two- and three-dimensional turbulent wakes. The analysis is valid for both near and far wakes. The only assumption involved in the analysis is the existence of similarity in velocity profiles. Based on this analysis, a computer program was written to predict the decay characteristics of wake-velocity defect and the variation of wake width downstream of the body. The numerical study includes wakes of a flat plate, airfoil, cascade of blades, and rotor blades. In all cases, results are in good agreement with experimental data. The simplicity, accuracy, and computational efficiency of this technique makes it very attractive.

Nomenclature

A = δ/L
C = chord length
C_E = Head's entrainment function
L = characteristic length scale of the wake (Fig. 1)
p^* = reduced pressure $[p - \rho(\Omega^2 r^2/2)]$
p = static pressure
Q_0 = total freestream velocity
r,θ,z = cylindrical coordinate system (Fig. 1)
s,n,r = coordinate system (Fig. 1); s is the projection of streamwise (freestream) coordinate on a cylindrical surface; n is the principal normal; r is the radial direction; $s = 0$ at the trailing edge, and $n = 0$ at the wake centerline
U,V,W = velocity components in s, n, r coordinate system (see Fig. 1)
W_c = maximum radial velocity
δ = semiwake width (Fig. 1)
δ_1, δ_2 = displacement thicknesses [Eq. (11)]
η = n/L_p, n/L_s
λ = stagger angle (angle between the chordline and the z direction)
Ω = angular velocity
τ = shear stress
$\theta_{11},\theta_{12},\theta_{22}$ = momentum thicknesses [Eq. (11)]

Subscripts

c = values at the wake centerline
d = defect in velocity [Eq. (14)]
e = edge values
R = reference values
s, p = suction and pressure surface

Received Nov. 26, 1986; presented as Paper 87-1437 at the AIAA 19th Fluid Dynamics, Plasma Dynamics, and Lasers Conference, Honolulu, HI, June 8-10, 1987; revision received Nov. 24, 1987.

*Evan Pugh Professor of Aerospace Engineering, Department of Aerospace Engineering. Fellow AIAA.
†Graduate Assistant, Department of Aerospace Engineering.

I. Introduction

TWO- and three-dimensional wakes encountered in fluid dynamics (wings, cylinders, turbomachinery rotors, etc.) belong to a class of complex turbulent flows. It is essential to develop a methodology to predict these wakes in order to understand their effect on aerodynamic loading and losses, unsteady forces, and noise generation. Practical examples in which such a prediction is essential are wake decay of an aircraft wing (so-called "wake turbulence" effect) and stator-rotor intractions (unsteady flow, noise) caused by the wakes of a preceding blade row in turbomachinery.

The analyses presently available for prediction of these wakes are valid in the far-wake region, where the history and nonisotropic effects are negligible. The methods available for two-dimensional wakes are described in Townsend.[1] No such analyses or predictive techniques are available for three-dimensional turbulent wakes such as those emerging from turbomachinery rotor blades, which are among the most complicated. They differ from isolated airfoil or cascade wakes in a number of ways: 1) the flow in the rotor wake is three-dimensional due to Coriolis and centrifugal forces and the three dimensionality of the blade row; 2) the flow is turbulent and the turbulence structure inside the blade boundary layer, which is shed out as a wake, is affected by rotation; and 3) the governing parameters of the rotor-wake characteristics include radial and axial pressure gradients, speed of rotation, blade and flow geometry, hub/tip ratio, and entry velocity profile, as well as freestream turbulence and distance from the trailing edge.

The objective of this research is to develop a technique for predicting wake development. The analysis is general and is valid for three-dimensional turbulent wakes. It includes the effects of curvature and rotation. It should enable calculation of unsteady forces caused by impingement of steady rotor wakes on a stator or interaction of a steady stator wake on a rotor (through frame of reference transformation). It should also enable acousticians to predict noise. Acousticians rely heavily on models developed for two-dimensional wakes, which become questionable when the wakes are three-dimensional.

Two methods are commonly used to calculate flow properties in the wake: the differential method and the momentum integral technique. The finite-difference technique is empoyed in the differential method to compute details of flow in the wake. Although this is necessary in understanding the nature

of the wake, the calculation is complex, time-consuming, and difficult to incorporate into design and analysis. The momentum integral technique, on the other hand, provides the gross properties of the wake. In most cases, this is all that is required in preliminary design, analysis, and estimation of wake effects. The momentum integral method provides a quick estimate of wake development and is easily coupled to other flow calculation routines. Lakshminarayana,[2] Cousteix et al.,[3] and Cousteix and Aupoix[4] made preliminary attempts to develop the momentum integral technique for three-dimensional wakes in rotor and wings, respectively. The present paper provides a generalized technique and a systematic approach for predicting both the two- and three-dimensional turbulent wakes with and without extra-strain effects such as curvature and rotation.

The present analysis is a new formulation, and the analysis is valid for the near wake as well as the far wake. The defect in velocities can be large in this formulation. The analysis and equations are presented in Sec. II, the numerical scheme in Sec. III, and the results in Sec. IV.

II. Analysis

Governing Equations

Assumptions made in the analysis of the rotor wake presented in this paper are listed below.

1) The approach is based on the boundary-layer approximation, neglects viscous-diffusion terms in the streamwise direction, and assumes that the freestream pressure gradient is superposed on the shear layer.

2) The analysis is applied along an assumed trajectory of the wake (usually the exit flow direction) and the position of the wake cannot be found as a part of the computation. The main emphasis here is to predict the wake width and the centerline velocity defect.

3) The interaction between the wake and the external flow is only through the prescription of the edge velocities. The analysis is not valid when the wakes of adjoining blades have merged.

4) The analysis is valid for incompressible flow, but the Mach number effects (all except shock wave phenomena) can be incorporated easily.

The most suitable coordinate system for the analysis of the rotor wake is the s,n,r system shown in Fig. 1. In the analysis, we assume the inviscid velocity vector to lie along a cylindrical surface. To keep the analysis general, the equations developed are for three-dimensional rotating wakes, including effects of curvature. The analysis, valid for nonrotating three- and two-dimensional wakes, is a simplified version of the general analysis.

The equations of mean motion in the coordinate system rotating with an angular velocity Ω is given by

Radial momentum equations (r):

$$W\frac{\partial W}{\partial r} + V\frac{\partial W}{\partial n} + U\frac{\partial W}{\partial s} + 2\Omega V\cos\lambda + 2\Omega U\sin\lambda - \frac{U^2}{r}\sin^2\lambda - \frac{V^2}{r}\cos^2\lambda = -\frac{1}{\rho}\frac{\partial p^*}{\partial r} + \frac{\partial}{\partial n}(\tau_{rn}) \tag{1}$$

where τ_{rn} is the turbulent stress in radial direction as shown in Fig. 1. Furthermore, p is the static pressure, and p^* is the reduced pressure.

$$p^* = p - \frac{\rho\Omega^2 r^2}{2}$$

The turbulence normal stresses are neglected in this equation. If the pressure gradient in the n direction is assumed to be very small (boundary-layer approximation), the following approximation can be made:

$$\frac{1}{\rho}\frac{\partial p_e^*}{\partial r} = \frac{1}{\rho}\frac{\partial p^*}{\partial r} = -2\Omega U_e\sin\lambda + \frac{U_e^2}{r}\sin^2\lambda$$

where p_e is the static pressure at the edge of the wake and U_e is the corresponding velocity. Hence, Eq. (1) reduces to

$$W\frac{\partial W}{\partial r} + V\frac{\partial W}{\partial n} + U\frac{\partial W}{\partial s} - 2\Omega(U_e - U)\sin\lambda + \frac{U_e^2 - U^2}{r}\sin^2\lambda = \frac{\partial}{\partial n}(\tau_{rn}) \tag{2}$$

Streamwise momentum equation (s):

$$U\frac{\partial U}{\partial s} + V\frac{\partial U}{\partial n} + W\frac{\partial U}{\partial r} - 2\Omega W\sin\lambda + \frac{UW}{r}\sin^2\lambda = U_e\frac{\partial U_e}{\partial s} + \frac{1}{\rho}\frac{\partial \tau_{sn}}{\partial n} \tag{3}$$

where τ_{sn} is the shear stress in the streamwise direction (Fig. 1). In Eq. (3), the streamwise pressure gradient term is replaced by $U_e(\partial U_e/\partial s)$. In Eqs. (1-3), only the dominant turbulent shear stress is retained; the normal component of turbulent stresses are neglected. Furthermore, W_e is assumed to be zero as the streamwise coordinate is aligned with the velocity vector in the freestream.

Continuity equation:

$$\frac{\partial U}{\partial s} + \frac{\partial V}{\partial n} + \frac{\partial W}{\partial r} + \frac{W}{r} = 0 \tag{4}$$

Momentum Integral Analysis

The essential differences between the momentum integral analysis for a boundary layer and a wake can be illustrated for two-dimensional flows (Ref. 4). Let s and n be streamwise and normal directions, with $W = 0$ and $\partial/\partial r = 0$. Then the continuity equation reduces to

$$\frac{\partial V}{\partial n} = -\frac{\partial U}{\partial s} \tag{5}$$

$$V = -\int_0^n \frac{\partial U}{\partial s} + C \tag{6a}$$

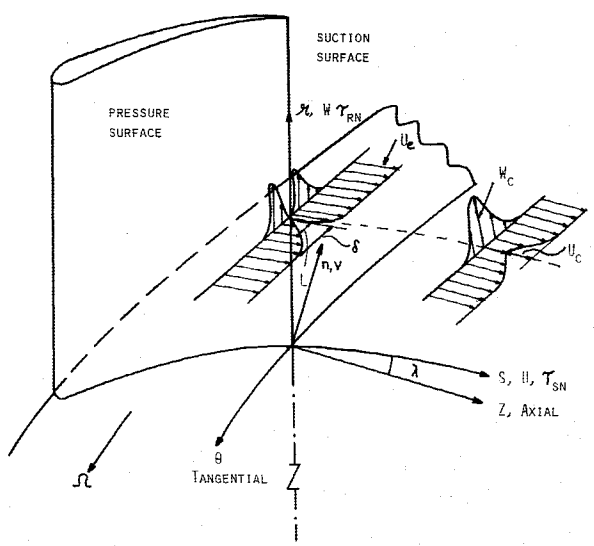

Fig. 1 Nature of rotor wake and notations used.

The velocity V is not zero at the wake centerline, hence

$$V = -\int \frac{\partial U}{\partial s} + V_c \tag{6b}$$

The appearance of V_c on the right-hand side of Eq. (6b) is the essential new element in the momentum integral analysis for a wake.

The momentum integral equation valid for a wake, in the most generalized case (three-dimensional rotating coordinate system), can be derived by integrating Eqs. (2) and (3) in the normal direction from the wake centerline to the wake edge. The integration is similar to those for three-dimensional boundary layer, as derived by Mager[5] and Anand and Lakshminarayana.[6] The difference between the momentum integral equation for the boundary layer and the wake arises in the values of the variables at the lower limit ($n = 0$). At $n = 0$, $U = V = W = 0$, and τ_{sn} and τ_{rn} are wall stresses in a boundary layer. In a wake, $u = U_c$, $V = V_c$, $W = W_c$, and $\tau_{sn} = \tau_{rn} = 0$ at $n = 0$ and δ. Here δ is the distance from the wake centerline to the freestream (Fig. 1). The velocity V in Eqs. (2) and (3) are eliminated using the continuity equation

$$V = -\int_0^n \left(\frac{\partial U}{\partial S} + \frac{\partial W}{\partial r} + \frac{W}{r}\right) dn + V_c$$

Typical integration of any quantity f (U, V, W, τ, etc.) and its derivatives can be classified as

$$\int_0^A \frac{\partial f(s,n,r)}{\partial n}\, dn = f(s,A,r) - f(s,0,r)$$

$$\int_0^A \frac{\partial f(s,n,r)}{\partial r}\, dn = \frac{d}{dr}\int_0^A f(s,n,r)\, dn - f(s,A,r)\frac{\partial A}{\partial r}$$

$$\int_0^A \frac{\partial f(s,n,r)}{\partial s}\, dn = \frac{d}{ds}\int_0^A f(s,n,r)\, dn - f(s,A,r)\frac{\partial A}{\partial s} \tag{7}$$

where $f(s,A,r)$ are $f(s,0,r)$ are the values of the function at the outer edge and centerline of the wake, respectively.

The integral momentum equations for a wake derived from the procedure described above is given by

s Momentum:

$$\frac{\partial \theta_{11}}{\partial s} + \frac{1}{U_e}\frac{\partial U_e}{\partial s}(2\theta_{11} + \delta_1) + \frac{1}{U_e}\frac{\partial U_e}{\partial r}(2\theta_{12} - \delta_2) + \frac{\partial}{\partial r}(\theta_{12}) + (\delta_2 \sin\lambda)\left\{\frac{2\Omega L}{U}\frac{1}{U_e} - \frac{\sin\lambda}{r}\right\} + \frac{1 + \sin^2\lambda}{r}\theta_{12} = \frac{V_c}{U_e}\left(1 - \frac{U_c}{U_e}\right) \tag{8}$$

r Momentum:

$$\frac{1}{r}\frac{\partial}{\partial r}(r\theta_{22}) + \frac{2\theta_{22}}{U_e}\frac{\partial U_e}{\partial r} + \frac{2}{U_e}\frac{\partial U_e}{\partial s}\theta_{21} + \frac{\partial \theta_{21}}{\partial s} + \theta_{11}\frac{\sin^2\lambda}{r} - \delta_1 \sin\lambda\left(\frac{2\Omega L}{U}\frac{1}{U_e} - \frac{\sin\lambda}{r}\right) = \frac{V_c W_c}{U_e^2} \tag{9}$$

Continuity:

$$\frac{\partial}{\partial s}[U_e(\delta - \delta_1)] + \frac{1}{r}\frac{\partial}{\partial r}(U_e r \delta_2) = U_e\frac{\partial \delta}{\partial s} + V_c - V_e \tag{10}$$

where U_e is the freestream velocity component derived from an inviscid solution and U_e and L are reference velocity and length scales, respectively. In Eqs. (8–10), all velocities are normalized by the reference velocity U_e, and the lengths (s, n,r,δ) are nondimensionalized by the length scale L. The momentum and displacement thicknesses are given by

$$\theta_{11} = \int_0^\delta \frac{U}{U_e}\left(1 - \frac{U}{U_e}\right] dn$$

$$\theta_{12} = \int_0^\delta \frac{W}{U_e}\left(1 - \frac{U}{U_e}\right) dn \tag{11a}$$

$$\theta_{21} = \int_0^\delta \frac{UW}{U_e^2}\, dn$$

$$\theta_{22} = \int_0^\delta \left(\frac{W}{U_e}\right)^2 dn \tag{11b}$$

$$\delta_1 = \int_0^\delta \left(1 - \frac{U}{U_e}\right) dn$$

$$\delta_2 = \int_0^\delta \frac{W}{U_e}\, dn \tag{11c}$$

If the wake is not symmetrical, the momentum, displacement, and boundary-layer thickness will be different on each wake. Thus, there will be two sets of Eqs. (8–10), one on each side of the wake. If the s direction is aligned with the streamline at the edge of the boundary layer, which is usually the case, $W_e = 0$.

The above integral equations, Eqs. (8–11), contain 10 unknowns, δ, δ_1, δ_2, θ_{11}, θ_{12}, θ_{21}, θ_{22}, V_c, W_c, and U_c, on each side of the wake. However, there are only three equations on each side of the wake. Hence, some simplifying assumptions must be made to couple various thicknesses in the equations. One of the simplifying assumptions that could be made is the velocity profile $U(n)$ and $W(n)$.

The existence of similarity in velocity profiles for two-dimensional wakes has been well-established (Ref. 1). Hah and Lakshminarayana[7] and Raj and Lakshminarayana[8] proved that the similarity in wake profiles exists both in the near wake and the far wake of insolated and cascade airfoils, respectively. The rotor wake data from Reynolds et al.[9] and Ravindranath and Lakshminarayana[10] also provide proof of the existence of similarity in velocity profiles for both U and W, in both the near and the far wake of a compressor rotor blade. Hence, the similarity in wake profile is assumed for both two- and three-dimensional wakes. The only region in which this assumption is not valid is very close to the trailing edge of a flat plate, airfoil, cascade blade, or rotor blade. This region is extremely complex, and no computation/analysis presently exists for the prediction of flows in this region. The similarity profiles are given by

$$\frac{U}{U_e} = 1 - U_d \exp(-0.693\,\eta^2) \tag{12}$$

$$\frac{W}{U_e} = \frac{W_c}{U_e}\exp(-0.693\,\eta^2) \tag{13}$$

where U_d is the nondimensionalized velocity defect given by

$$U_d = 1 - \frac{U_c}{U_e}$$

and

$$\eta = \frac{n}{L_p}$$

or

$$\eta = \frac{n}{L_s} \tag{14}$$

where L_p and L_s are wake widths at half the depth $[(U_e - U_c)/2]$ of the U velocity profile defect on the pressure side and suction side, respectively. This is the length scale mentioned earlier (Fig. 1). In what follows, L indicates L_s or L_p depending on the pressure side or suction side of the wake.

The assumptions for velocity provides [Eqs. (12) and (13)] are based on the similarity analysis of the rotor wake data carried out by Reynolds et al.[9] and Ravindranath and Lakshminarayana.[10] The assumptions for the streamwise velocity profile [Eq. (12)] is based on extensive analysis of two-dimensional wake data by Townsend[1] and others. The theoretical and physical reasoning for the choice of these profiles can be found in Refs. 1, 7, 9, and 10.

Substituting Eqs. (12) and (13) into Eq. (11), the various thicknesses can be expressed in terms of velocity defects as

$$\theta_{11} = L\frac{U_d}{U_e}\left[1.06 - 0.753\frac{U_d}{U_e}\right] \tag{15a}$$

$$\theta_{12} = 0.753\,L\frac{W_c}{U_e}\frac{U_d}{U_e}, \quad \theta_{22} = 0.753\frac{LW_c^2}{U_e^2} \tag{15b}$$

$$\theta_{21} = L\left(1.06\frac{W_c}{U_e} - 0.753\frac{U_d}{U_e}\frac{W_c}{U_e}\right) \tag{15c}$$

$$\delta_1 = 1.06\,L\frac{U_d}{U_e}, \quad \delta_2 = 1.06\,L\frac{W_c}{U_e} \tag{15d}$$

Substituting Eq. (10) into Eqs. (8) and (9) to eliminate V_c, and using Eqs. (15a–15d), we arrive after considerable manipulation at the following equations.

r Momentum equation:

$$\left(1.06 + 0.307\frac{U_d}{U_e}\right)\frac{W_c}{U_e}\frac{\partial L}{\partial s} + 0.307\,L\frac{W_c}{U_e}\frac{\partial}{\partial s}\left(\frac{U_d}{U_e}\right) + L\left(1.06 - 0.753\frac{U_d}{U_e}\right)\frac{\partial}{\partial s}\left(\frac{W_c}{U_e}\right)$$
$$= -\frac{\sin^2\lambda}{r}\theta_{11} - \frac{1}{r}\frac{\partial}{\partial r}(r\theta_{22}) - \frac{2}{U_e}\frac{\partial U_e}{\partial r}\theta_{22} - \frac{2}{U_e}\frac{\partial U_e}{\partial s}\theta_{21} + \delta_1\sin\lambda\left[\left(\frac{2\Omega L}{U}\right)\frac{1}{U_e} - \frac{\sin\lambda}{r}\right]$$
$$+ \frac{W_c}{U_e}\left[\frac{1}{U_e}\frac{\partial U_e}{\partial s}(AL - \delta_1) + \frac{1}{r}\frac{\partial}{\partial r}(r\delta_2) + \frac{\partial U_e}{\partial r}\frac{\delta_2}{U_e}\right] \tag{16}$$

s Momentum equation:

$$\frac{U_d}{U_e}\left(1.06 + 0.307\frac{U_d}{U_e}\right)\frac{\partial L}{\partial s} + L\left(1.06 - 0.446\frac{U_d}{U_e}\right)\frac{\partial}{\partial s}\left(\frac{U_d}{U_e}\right)$$
$$= \frac{U_d}{U_e}\left[\frac{1}{U_e}\frac{\partial U_e}{\partial s}(AL - \delta_1) + \frac{1}{r}\frac{\partial}{\partial r}(r\delta_2) + \frac{1}{U_e}\frac{\partial U_e}{\partial r}\delta_2\right]$$
$$- \frac{1}{U_e}\frac{\partial U_e}{\partial s}(2\theta_{11} + \delta_1) - \frac{\partial\theta_{12}}{\partial r} - \frac{1}{U_e}\frac{\partial U_e}{\partial r}(2\theta_{12} - \delta_2)$$
$$- \left[\left(\frac{2\Omega L}{U}\right)\frac{1}{U_e} - \frac{\sin\lambda}{r}\right]\delta_2\sin\lambda - \left(\frac{\sin^2\lambda + 1}{r}\right)\theta_{12} \tag{17}$$

On each side of the wake, there are two equations, Eqs. (16) and (17), for three unknowns, L, U_d, and W_c. For a symmetrical wake, the equations are identical on both sides. Values θ_{11}, θ_{12}, θ_{21}, etc., can be derived from Eqs. (15), using the known values of L, U_d, and W_c. An additional closure equation is needed to complete the set of equations for prediction of these three unknowns.

Closure Model

The entrainment equation, derived by Head,[11] is used as a closure model. The concept is based on the fact that a turbulent shear layer grows by a proces of "entrainment" of inviscid fluid at the edge of the shear layer. The entrainment equation by Head has been extended by Nash and Patel[12] for a three-dimensional flow. The approach adopted here is similar to that of Anand and Lakshminarayana,[6] Cousteix et al.,[3] and Cousteix and Aupoix.[4] The entrainment equation can be written as

$$\frac{1}{U_e}\frac{\partial}{\partial s}[U_e(\delta - \delta_1)] - \frac{1}{U_e r}\frac{\partial}{\partial r}(U_e r\delta_2) = C_E(H) + \frac{V_c}{U_e} \tag{18}$$

where C_E is Head's entrainment function [terms $U_e(\partial\delta/\partial s) - V_e$ in Eq. (10)] and $H = (\delta - \delta_1)/\theta_{11}$. The entrainment function C_E represents the volume flow rate per unit area through the surface of the wake edge, and is the rate of entrainment of inviscid external flow into the wake.

The entrainment process is a highly complex and inherently unsteady phenomena and its direct measurement is difficult. The entrainment rate depends on many flow parameters, such as streamwise velocity defect, rate of growth of wake width, freestream velocity, displacement thickness, etc. An empirical correlation for the entrainment function C_E for three-dimensional flows is not yet available, expecially for a three-dimensional rotor wake flow. Hence, the entrainment function C_E of Head[11] for two-dimensional boundary-layer flow is used in the present analysis. The function is given by

$$C_E(H) = C_1\,(H - 3.0)^{-0.653} \tag{19}$$

where $C_1 = 0.0306$. It is obvious that this function is subject to modification for the wake flow. Equations (16–19) can be solved in each side of the wake to establish U_c, W_c, and L. To start the computation, the three-dimensional inviscid-flow velocity U_e is needed that can be derived from an inviscid-flow computation or experimental data. The initial condition at the trailing edge (L_s, L_p, U_c, W_c) is prescribed according to a boundary-layer computation or experimental data.

Matching and Boundary Conditions

The values of U_c, W_c, and V_c should be identical for both sides of the wake, even though the values of U_e and L may be different. Thus, there are six equations (three on each side) for five unknowns, U_c, W_c, V_c, L_s, and L_p. The additional equation will generate different values for the centerline velocity. To satisfy the boundary condition at the wake centerline (i.e., V_c, U_c, W_c must be identical for both sides of the wake), the principal equation [Eq. (17)] on each side of the wake is combined to provide a single equation for U_c.

The procedure used for satisfying the matching condition for the wake is as follows: 1) Identical values of V_c are used on either side of the wake in Eq. (10) to derive a composite expression for V_c that contains the parameters from both sides

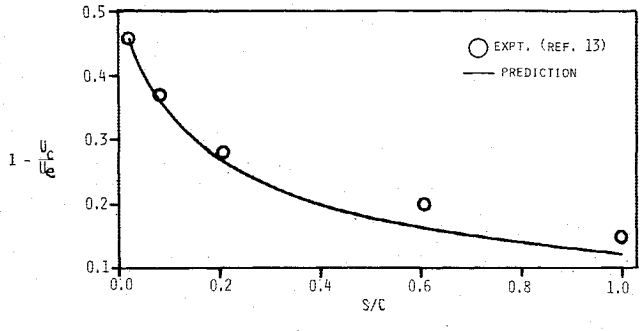

Fig. 2 Decay of the defect in centerline velocity in the wake of a flat plate.

of the wake. 2) The composite expression for V_c is substituted in Eq. (8) for both the pressure and the suction sides of the wake. These momentum equations are then added to derive a composite principal equation for the wake. This composite expression, given below, satisfies the matching condition for U_c and V_c. 3) The matching condition for W_c is enforced in Eq. (16) by assuming identical values of W_c on either side of the wake,

$$\left(1-\frac{U_c}{U_{ep}}\right)\left[0.307+0.753\,\frac{U_c}{U_{ep}}+0.53\left(1-\frac{U_c}{U_{ep}}+\frac{U_{ep}}{U_{es}}-\frac{U_c}{U_{ep}}\frac{U_{ep}^2}{U_{es}^2}\right)\right]\frac{\partial L_p}{\partial s}-\left\{L_p\left(1.506\,\frac{U_c}{U_{ep}}-0.446\right)+L_s\left(1.506\,\frac{U_{ep}}{U_{es}}\frac{U_c}{U_{ep}}-0.446\right)\times\frac{U_{ep}}{U_{es}}-\left(1-\frac{U_c}{U_{ep}}+\frac{U_{ep}}{U_{es}}-\frac{U_c}{U_{ep}}\frac{U_{ep}}{U_{es}}\right)\left(L_p+L_s\,\frac{U_{es}}{U_{ep}}\right)0.53\right\}\times\frac{\partial}{\partial s}\left(\frac{U_c}{U_{ep}}\right)+\left\{\left(1-\frac{U_c}{U_{ep}}\frac{U_{ep}}{U_{es}}\right)\left(0.307+0.753\,\frac{U_c}{U_{ep}}\frac{U_{ep}}{U_{es}}\right)+0.53\,\frac{U_{es}}{U_{ep}}\left(1-\frac{U_c}{U_{ep}}\frac{U_{ep}}{U_{es}}\right)\left(1-\frac{U_c}{U_{ep}}+\frac{U_{ep}}{U_{es}}-\frac{U_c}{U_{ep}}\frac{U_{ep}^2}{U_{es}^2}\right)\right\}\frac{\partial L_s}{\partial s}$$

$$=L_s\,\frac{U_c}{U_{ep}}\left[\left(1.506\,\frac{U_{ep}}{U_{es}}\frac{U_c}{U_{ep}}\right)+\left(1-\frac{U_c}{U_{ep}}+\frac{U_{ep}}{U_{es}}-\frac{U_c}{U_{ep}}\frac{U_{ep}^2}{U_{es}^2}\right)\times 0.53\,\frac{U_{es}}{U_{ep}}\right]\left(\frac{1}{U_{es}}\frac{\partial U_{ep}}{\partial s}-\frac{U_{ep}}{U_{es}^2}\frac{\partial U_{es}}{\partial s}\right)+\frac{1}{2}\left(1-\frac{U_c}{U_{ep}}+\frac{U_{ep}}{U_{es}}-\frac{U_c}{U_{ep}}\frac{U_{ep}^2}{U_{es}^2}\right)\left[\left(A_p\,L_p-\delta_{1p}\right)\frac{1}{U_{ep}}\frac{\partial U_{ep}}{\partial s}+\left(A_sL_s-\delta_{1s}\right)\frac{1}{U_{ep}}\times\frac{\partial U_{es}}{\partial s}+\frac{\partial\delta_{2p}}{\partial r}+\frac{\delta_{2p}}{r}+\frac{U_{es}}{U_{ep}}\frac{\partial\delta_{2s}}{\partial r}+\frac{U_{es}}{U_{ep}}\frac{\delta_{2s}}{r}+\frac{\delta_{2p}}{U_{ep}}\frac{\partial U_{ep}}{\partial r}+\frac{\delta_{2s}}{U_{ep}}\frac{\partial U_{es}}{\partial r}\right]-\frac{1}{U_{ep}}\frac{\partial U_{ep}}{\partial s}\left[2(\theta_{11})_p+\delta_{1p}\right]-\frac{1}{U_{es}}\frac{\partial U_{es}}{\partial s}\times\left[2(\theta_{11})_s+\delta_{1s}\right]-\frac{\partial(\theta_{12})_p}{\partial r}-\frac{\partial(\theta_{12})_s}{\partial r}-\frac{1}{U_{ep}}\frac{\partial U_{ep}}{\partial r}\times\left[2(\theta_{12})_p-\delta_{2p}\right]-\frac{1}{U_{es}}\frac{\partial U_{es}}{\partial r}\left[2(\theta_{12})_s-\delta_{2s}\right]-\frac{2\Omega L}{U}\sin\lambda\times\left(\frac{\delta_{2p}}{U_{ep}}+\frac{\delta_{2s}}{U_{es}}\right)+\frac{\sin^2\lambda}{r}\left(\delta_{2p}+\delta_{2s}\right)-\frac{\sin^2\lambda+1}{r}\times\left[(\theta_{12})_p+(\theta_{12})_s\right] \tag{20}$$

This equation satisfies the condition that U_c is the same for both sides of the wake. Similarly, the combined entrainment equation can be obtained. This is given by

$$\left[A_p-0.53\left(1-\frac{U_c}{U_{ep}}\right)\left(\frac{U_{ep}}{U_{es}}+1\right)\right]\frac{\partial L_p}{\partial s}+0.53\times\left[L_p-L_s+\frac{U_{ep}}{U_{es}}\left(L_p+3L_s\right)\right]\frac{\partial}{\partial s}\left(\frac{U_c}{U_{ep}}\right)+\left[A_s+0.53\left(1-\frac{U_c}{U_{ep}}\frac{U_{ep}}{U_{es}}\right)\left(\frac{U_{es}}{U_{ep}}-3\right)\right]\frac{\partial L_s}{\partial s}=C_{Ep}+C_{Es}+0.53\,L_s\,\frac{U_c}{U_{ep}}\left(\frac{1}{U_{es}}\frac{\partial U_{ep}}{\partial s}-\frac{U_{ep}}{U_{es}^2}\frac{U_{es}}{\partial s}\right)\left(\frac{U_{es}}{U_{ep}}-3\right)+\frac{\partial(\delta_{2p})}{\partial r}+\frac{\partial(\delta_{2s})}{\partial r}+\frac{\delta_{2p}}{U_{ep}}\frac{\partial U_{ep}}{\partial r}+\frac{\delta_{2s}}{U_{es}}\frac{\partial U_{es}}{\partial r}+\frac{\delta_{2p}}{r}+\frac{\delta_{2s}}{r}-\frac{1}{2}\left(\frac{1}{U_{ep}}+\frac{1}{U_{es}}\right)\left(A_pL_p-\delta_{1p}\right)\times\frac{\partial U_{ep}}{\partial s}-\frac{1}{2}\left(\frac{1}{U_{ep}}-\frac{3}{U_{es}}\right)\times\left(A_sL_s-\delta_{1s}\right)\times\frac{\partial U_{es}}{\partial s}+\frac{1}{2}\left(1-\frac{U_{ep}}{U_{es}}\right)\left(\frac{\partial\delta_{2p}}{\partial r}+\frac{U_{es}}{U_{ep}}\frac{\partial\delta_{2s}}{\partial r}+\frac{\delta_{2p}}{U_{ep}}\frac{\partial U_{ep}}{\partial r}+\frac{\delta_{2s}}{U_{ep}}\frac{\partial U_{es}}{\partial r}+\frac{\delta_{2p}}{r}+\frac{U_{es}}{U_{ep}}\frac{\delta_{2s}}{r}\right) \tag{21}$$

Equations (20) and (21), together with pressure side and suction side radial momentum equation, Eq. (16), (with the same value for W_c) constitute a closed set of equations for determining the variables U_c, W_c, L_p, and L_s for the entire wake.

III. Numerical Scheme

The Gill variation of the Runge-Kutta fourth-order scheme is used to integrate Eqs. (16), (20), and (21) in the streamwise direction. A centered-difference approximation is used for the radial derivative. The method is an explicit scheme in that the radial derivatives are lagged in the calculation. The four-step Runge-Kutta method allows the radial derivative to be corrected at each half-step of the calculation.

The values of $U_{ep}(s,r)$ and $U_{es}(s,r)$ can be specified either by using an inviscid solver or from experimental data. In most cases, the variation of U_{ep} and U_{es} with s is small and their variation with the radius is similar to that at the trailing edge.

The wake width at $s = 0$ is the boundary-layer thickness at the trailing edge that can be derived from either a boundary-layer prediction scheme or boundary-layer measurement. The inviscid-flow code, the boundary-layer code, and the wake code can be coupled together to form a complete flowfield prediction technique.

Either the initial value of the streamwise velocity U_c at the trailing edge is specified as zero or the measured value is used from the first measuring station. The boundary condition for the radial velocity presents some difficulty. The value of W_c at the trailing edge is zero; but in the similarity relationship for the radial velocity, W_c cannot be zero. Therefore, the measured value from the first measuring station was used for the rotor wake. In a rotor wake, the peak radial velocities occur away from the wake centerline. The highest value of the radial velocity is used as the initial value in the calculation. Since these two radial velocity peaks are close to and symmetric with the wake centerline, the error due to this approximation should be small. In fact, as the wake develops further downstream, these two radial velocity peaks join, which improves the accuracy of the approximation.

The numerical scheme showed no instability in the test cases for which the program was run. The convergence of the solution was very rapid. The run time on an IBM 3033 computer for two-dimensional cases was about 5 s, and for three-dimensional cases about 15 s.

IV. Results and Interpretation

The method of analysis decribed earlier was used to predict the decay of the wakes from a flat plate,[13] an isolated airfoil,[14] a three-dimensional wing,[3] a cascade,[8] and compressor and fan rotor blades.[9,10] The prediction for the two-dimensional case (flat plate, airfoil, and cascade) includes only the streamwise pressure gradient or the edge velocity gradient $\partial U_e/\partial s$. This, as well as the radial velocity gradient $\partial U_e/\partial r$, is a requirement for rotor-wake prediction.

The coefficient C_1(= 0.0306) is Eq. (19), given by Head,[11] is valid for two-dimensional boundary layers. In the near-wake region, the entrainment is likely to be higher. Furthermore, the entrainment occurs on both edges of a wake compared to a boundary layer, in which the entrainment occurs on only one side. Hence, the initial computations based on the assumed

value for the coefficient C_1 in Eq. (19) were not accurate. Doubling this coefficient provided good predictions for both the flat-plate wake and the wake of an isolated airfoil. Analysis of the far wake by Nakayama et al.[15] indicates that this coefficient is about two to three times that used for a boundary layer.

The cascade wake and rotor wake develop internally under the constraint of adjoining blades. The flows in these cases and in the case of a three-dimensional wing are much more complex than simple two-dimensional shear flows. The coefficient C_1 in this case had to be increased to 0.2142 in order to obtain good predictions. This introduces an additional concept, namely, that each class of flows requires a differeing entrainment coefficient. All external-flow wake predictions (flate, isolated airfoil) were done with a coefficient equal to 0.0612. All internal flows (cascades and turbomachinery rotor wakes) and three-dimensional wakes were done with a coefficient of 0.2142. Since the coefficients were changed according to geometry and flow type rather than being changed for each case, the method is accurate and reliable, and it should be applicable to all wake flows.

The wake prediction was also found to be very sensitive to the values of $\partial U_e/\partial s$ and $\partial U_e/\partial r$, especially in the case of cascade wake and rotor wake. These were specified from the inviscid data measured away from the wake.

Two-Dimensional Wake

The prediction of a flat-plate wake, measured by Chevray and Kovasznay,[13] is shown in Figs. 2 and 3. The wake in this case is symmetrical, and $U_{ep} = U_{es}$, $L_s = L_p$. The initial value of U_c and L were derived from the measured data at the first station located at the trailing edge ($s = 0$). It should be noted here that the predictions are carried out with only one empirical constant in the equation and the agreement between the data and the predictions is excellent.

Yu[14] has provided a comprehensive set of data for the near wake of an isolated airfoil (NACA 53-012) at zero incidence (hence, $L_s = L$, $U_{ep} = U_{es}$). The boundary-layer measurements were carried out at nine chordwise locations in the last 10% of blade chord; the wake was measured at eight axial locations within 10% of blade chord from the trailing edge. This data provides a critical test on the applicability of the analysis to near-wake flows. The data $X = 1.0029$ (0.29% of chord from trailing edge) was used to establish the initial conditions. The variation of the wake width and the velocity defect with distance are predicted accurately, as shown in Figs. 4 and 5, respectively.

For internal flows, one of the critical tests of any model is the prediction of the wake from a cascade of blades and rotor blades. The wakes in a cascade develop in the presence of other wakes as well as a streamwise pressure gradient $\partial U_e/\partial s$. The data acquired by Raj and Lakshminarayana[8] in a cascade of airfoils at 0- and 2-deg incidence is compared with the predictions from the present analysis in Figs. 6 and 7. The cascade consisted of seven blades, with a chord to space of 1.505, inlet angle of 45 deg, and Reynolds number (based on chord) of 3.2×10^5. The experimental data at the trailing edge was used as initial conditions for the prediction. In both 0- and 2-deg incidence cases, the predictions for the decay of the defect in the centerline velocity is excellent. The wake width is predicted well except very close to the trailing edge.

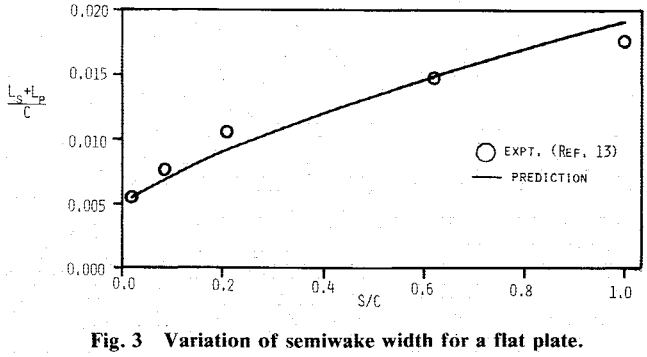

Fig. 3 Variation of semiwake width for a flat plate.

Three-Dimensional Wakes

The predictions based on the present analysis are compared with the data measured by Cousteix et al.[3] and Cousteix and Aupoix[4] for a three-dimensional wake of a wing, the fan rotor

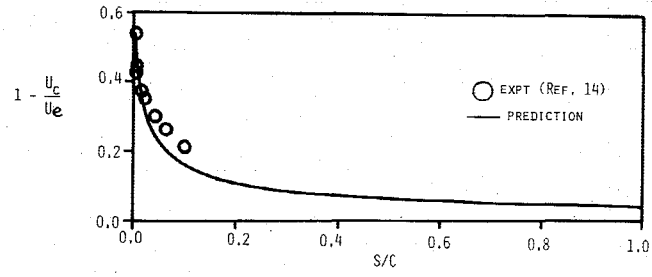

Fig. 4 Decay of the defect in wake centerline velocity for an isolated airfoil.

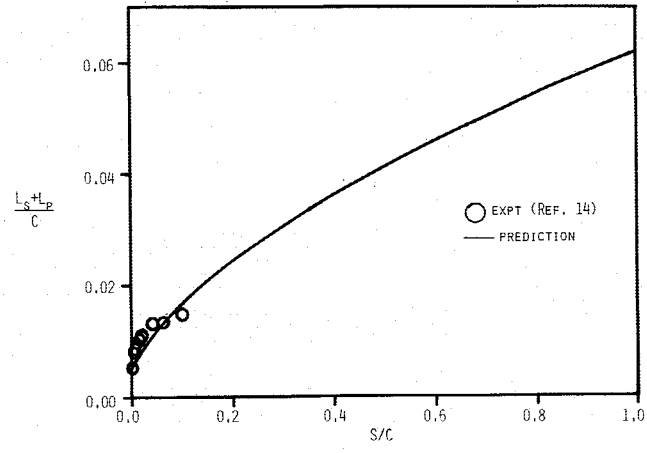

Fig. 5 Semiwake width variation for an isolated airfoil.

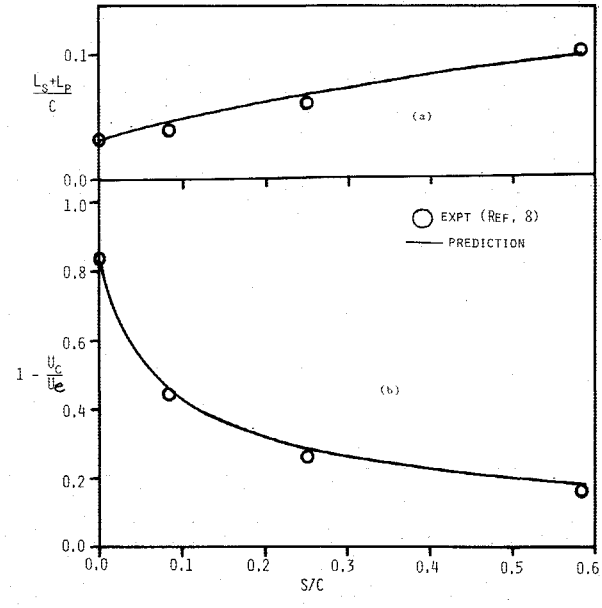

Fig. 6 Variation of wake properties for a cascade at 0-deg incidence: a) semiwake width; b) decay of defect in centerline velocity.

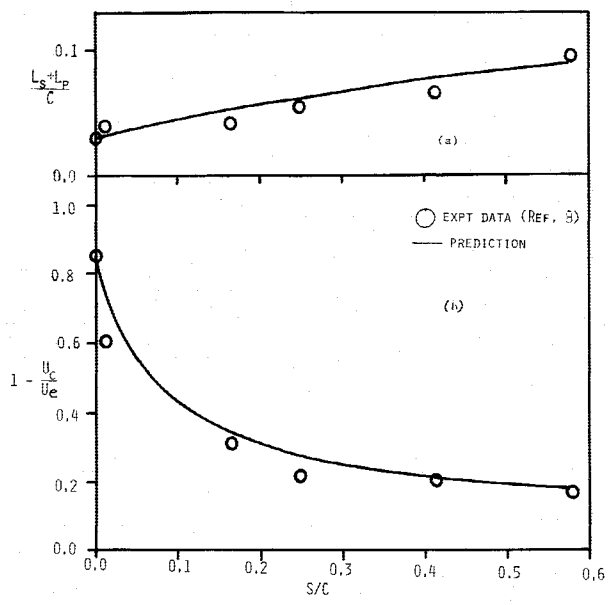

Fig. 7 Variation of wake properties for a cascade at 2-deg incidence; a) semiwake width; b) decay of defect in centerline velocity.

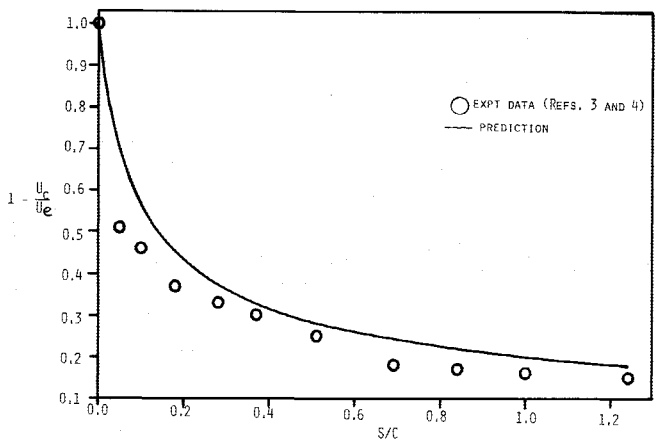

Fig. 8 Decay of the defect in the mainstream centerline velocity for the wake of a swept wing.

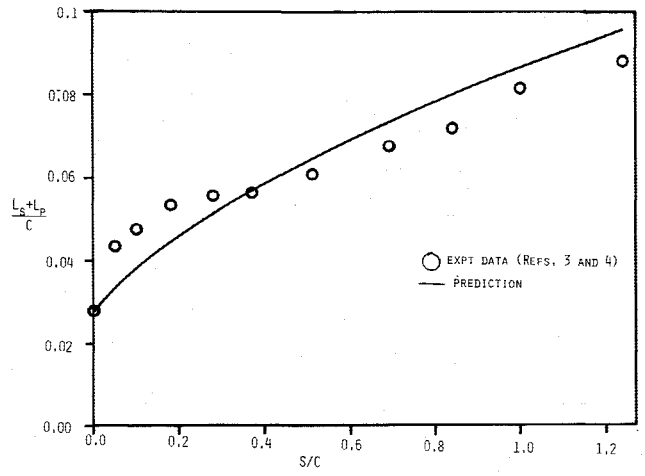

Fig. 9 Variation of semiwake width for the wake of a swept wing.

wake data of Reynolds et al.,[9] and the compressor rotor wake data of Ravindranath and Lakshminarayana.[10]

Cousteix el at.[3] and Cousteix and Aupoix[4] conducted detailed measurements of the three-dimensional wake of a swept wing in a subsonic stream. The wing section used was an ONERA D profile. The chord length was constant and equal to 200 mm. The swept angle was 22.5 deg, and the angle of attack was 8 deg. The freestream velocity was 35 m/s, providing a Reynolds number of 4.7×10^5 based on the chord length. The measurement was carried out up to a distance of 1.24 chord length from the trailing edge. As the wake in this case is three-dimensional and asymmetric, this experimental data can be used to check the validity of the code for three-dimensional flows and the applicability of the matching technique discussed earlier. The experimental data at the trailing edge is used as the starting condition for the computation. The comparison between the experiment and the computation shows that the decay in defect in central velocity (Fig. 8) and the wake width (Fig. 9) are predicted very well, except very near the trailing edge. Considering that the radial velocity at the centerline W_c is small, the predictions are quite satisfactory (Fig. 10). The results indicate that the momentum integral technique provides good prediction of three-dimensional wakes.

The wake of a compressor or fan rotor is one of the most complex shear flows encountered in practice. As indicated earlier, the extra-strain effect caused by the Coriolis forces and centerifugal forces as well as the radial pressure gradient $\partial U_e/\partial r$ introduces considerable three-dimensionality into the wake structure. Reynolds et al.[9] measured the wake of an axial-flow fan rotor blade. The fan had a tip diameter of 54.6 cm, hub diameter of 24.1 cm, blade chord of 15.2 cm, and space-to-chord ratio (midspan) of 0.68; the blading consisted of British C_1 profile. The wake properties measured at the midradius and at an incidence of 10 deg is shown compared with predictions in Fig. 11. Because of lack of experimental data at other radii, the initial condition is assumed to be the same for all the radii, i.e., the measured values near the trailing edge at the midradius were used as initial conditions for the prediction. Considering the complex nature of the flow, agreement between the data and the prediction is excellent for the defect along the centerline of the streamwise velocity, radial velocity, and the wake width.

Ravindranath and Lakshminarayana[10] measured the wake from a heavily loaded compressor blade. The compressor had 21 NASA-65 series blades, and a tip diameter of 0.932 m ($R = 1$) with a hub-tip ratio of 0.5. The blade chord at midspan was 13.46 cm with a spacing of 10.52 cm. The analysis developed in this paper does not take into account the

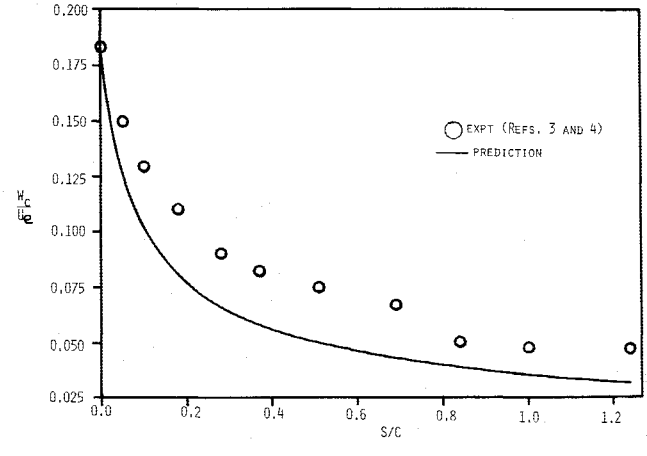

Fig. 10 Decay of the maximum spanwise velocity in the wake of a swept wing.

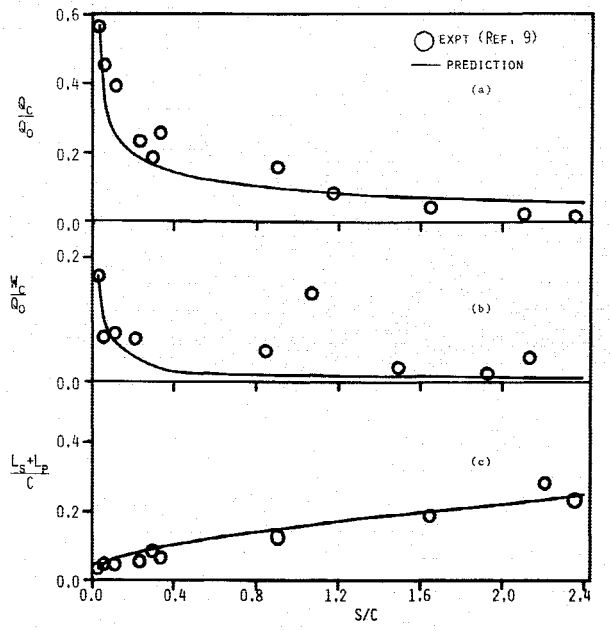

Fig. 11 Predicted and measured variation in wake properties of a fan rotor: a) decay in defect in total centerline velocity Q_c; b) decay of maximum radial velocity W_c; c) variation of semiwake width, (Q_0 is the total freestream velocity, the wake properties are at 10-deg incidence, at non-dimensionalized radius $R = 0.721$).

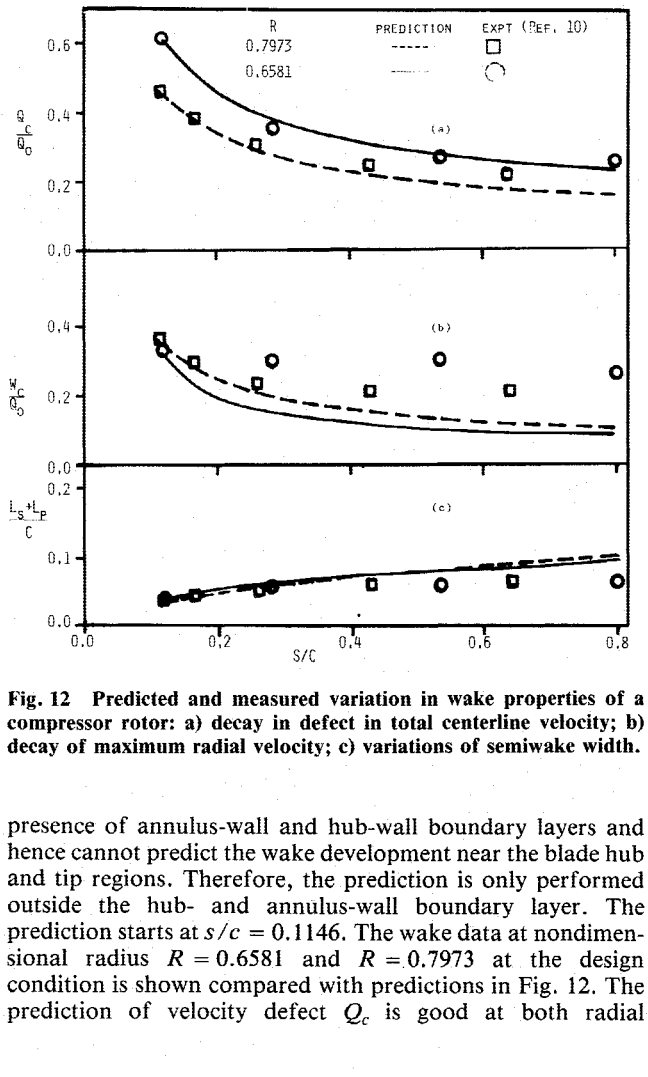

Fig. 12 Predicted and measured variation in wake properties of a compressor rotor: a) decay in defect in total centerline velocity; b) decay of maximum radial velocity; c) variations of semiwake width.

presence of annulus-wall and hub-wall boundary layers and hence cannot predict the wake development near the blade hub and tip regions. Therefore, the prediction is only performed outside the hub- and annulus-wall boundary layer. The prediction starts at $s/c = 0.1146$. The wake data at nondimensional radius $R = 0.6581$ and $R = 0.7973$ at the design condition is shown compared with predictions in Fig. 12. The prediction of velocity defect Q_c is good at both radial locations. The radial velocity predictions are poor, especially for $R = 0.6581$. The prediction of the wake width is good, expecially for the near wake. It is quite likely that the influence of the hub-wall boundary layer, neglected in this analysis, may be responsible for the discrepancy observed at $R = 0.6581$, especially for the radial velocity prediction. The wake of a heavily loaded compressor rotor is one of the most complex wakes in fluid mechanics, and the ability of the momentum integral analysis to predict this wake seems to indicate that the present analysis is very useful in predicting the two- and three-dimensional complex wakes encountered in practice.

V. Concluding Remarks

The momentum integral technique presented here for predicting both two- and three-dimensional turbulent wakes is accurate. A better entrainment model based on three-dimensional considerations is needed for improvements in the present analysis. The simplicity and accuracy of the method is very attractive compared to the complete numerical solution based on relaxation or time-marching methods which require complex coding and several orders of magnitude more computational time. The method seems to capture the decay properties and essential physics of wakes in both internal and external flows.

References

[1]Townsend, A. A., *The Structure of Turbulent Shear Flow*, Cambridge Univ. Press, Cambridge, England, U.K., 1956.

[2]Lakshminarayana, B., "The Nature of Flow Distortions Caused by Rotor Blade Wakes," AGARD CP-177, 1976.

[3]Cousteix, J., Pailhas, G., and Aupoix, B., "Three-Dimensional Wake of a Swept Wing," *Proceedings of the 2nd Symposium on Physical Aspects of Aerodynamic Flows*, edited by T. Cebeci, Univ. of California, Long Beach, CA, Jan. 1983.

[4]Cousteix, J. and Aupoix, B., "An Integral Method for Calculating a Three-Dimensional Wake," Fiche Technique, Office National L'Etudes et de Recherches Aeronautiques, Toulouse, France, Rept. No. 2, 1983.

[5]Mager, A., "Generalizations of Boundary-Layer Momentum Integral Equations to Three-Dimensional Flow Including Rotating Systems," NACA Rept. 1067, 1952.

[6]Anand, A. K. and Lakshminarayana, B., "Three Dimensional Turbulent Boundary Layer in a Rotating Helical Channel," *Journal of Fluids Engineering*, Vol. 97, 1975, p. 197.

[7]Hah, C. and Lakshminarayana, B., "Measurement and Prediction of Mean Velocity and Turbulence Structure in the Near Wake of an Airfoil," *Journal of Fluid Mechanics*, Vol. 115, 1982, p. 251.

[8]Raj, R. and Lakshminarayana, B., "Characteristics of the Wake Behind a Cascade of Aerofoils," *Journal of Fluid Mechanics*, Vol. 61, 1973, p. 707.

[9]Reynolds, B., Lakshminarayana, B., and Ravindranath, A., "Characteristics of the Near Wake of a Compressor Rotor," *AIAA Journal*, Vol. 17, Sept. 1979, pp. 959–967 (also see NASA CR-3188, Oct. 1979).

[10]Ravindranath, A. and Lakshminarayana, B., "Mean Velocity and Decay Characteristics of the Near- and Far-Wake of a Moderately Loaded Compressor," ASME, *Journal of Engineering Power*, Vol. 102, 1980, p. 535.

[11]Head, M. R., "Entrainment in the Turbulent Boundary Layers," British Aeronautical Research Council, R&M 3152, 1958.

[12]Nash, J. F. and Patel, V. C., *Three Dimensional Turbulent Boundary Layers*, Scientific and Business Consultants Inc., Atlanta, GA, 1972.

[13]Chevray, R. and Kovasznay, L. S. G., "Turbulent Measurements in the Wake of a Thin Flat Plate," *AIAA Journal*, Vol. 7, Aug. 1969, pp. 1641–1642.

[14]Yu, J. C., "Mean and Turbulence Measurements in the Vicinity of the Trailing Edge of an NACA 63-012 Airfoil," NACA TP-1985, 1981.

[15]Nakayama, A., Patel, V. C., and Landweber, L., "Flow Interaction Near the Tail of a Body of Revolution, Part 2," *Journal of Fluids Engineering*, Vol. 98, p. 538.